A biphenol-based chemosensor for Zn(II) and Cd(II) metal ions: synthesis, potentiometric studies and crystal structures

Gianluca Ambrosi,[a] Mauro Formica,[a] Vieri Fusi,*[a] Luca Giorgi,*[a] Eleonora Macedi,[b] Mauro Micheloni,[a] Paola Paoli,*[c] Patrizia Rossi.[c]

[a]*Department of Pure and Applied Sciences, University of Urbino, P.zza Rinascimento 6, I-61029 Urbino, Italy. Tel/Fax: +39-0722-350032. Email: luca.giorgi@uniurb.it*

[b]*Department of Chemistry and Biology University of Salerno, via Giovanni Paolo II 132,I-84084 Fisciano (SA), Italy.*

[c]*Department of Industrial Engineering, University of Florence, via S. Marta 3, I-50139 Florence, Italy.*

Keywords: Biphenol / Synthesis / Potentiometric studies / X-ray structures

Abstract

We synthesized and characterized the ligand N,N'-Bis[(2,2'-dihydroxybiphen-3-yl)methyl]-N,N'-dimethylethylenediamine (**L**), which contains two biphenol moieties (BPH) linked as side arms to an N,N'-dimethylethylenediamine scaffold. The ligand is highly soluble in a water/ethanol 50/50 v/v mixture and, in its deprotonated form $H_{-2}\mathbf{L}^{2-}$, is able to coordinate transition metal ions such as Ni(II), Zn(II), Cu(II), Cd(II) and Pd(II). Crystal structures of [Ni(H_{-2}**L**)·2(*n*-BuOH)], [Ni(H_{-2}**L**)·2(MeOH)], [Cd(H_{-2}**L**)·2(DMF)], [Cu(H_{-2}**L**)(DMF)] and [Pd(H_{-2}**L**)(DMF)] were also determined and described. Potentiometric titrations were carried out in mixed solvent with Zn(II), Cu(II) and Ni(II) metal ions to determine the acid-base and stability constants. **L** was

highly fluorescent in the visible range (400 nm). Moreover, its emission intensity increased upon the addition of Zn(II) or Cd(II) ions in an ethanol/water solution, and behaved as a chemosensor for the presence of these ions in the solution.

Introduction

Transition metal complexes have important roles that span material to medicinal chemistry, which are two of the main interesting applications in advanced chemical research. In fact, metal complexes are used as building blocks to produce new surfaces and nanostructures in supramolecular chemistry,[1] and they play a central part in medicinal chemistry as they are commonly used as model systems for the active centres of many metalloenzymes.[2] In addition, they can be used as devices to host and carry small molecules or ions of pharmaceutical and physiological interest, as well as chemotherapeutic agents[3,4]. In organic synthesis and analytical chemistry, metal complexes can be used as catalysts[5] and in the development of optical sensors for the detection of in-trace analytes.[6]

In view of this, the synthesis of ligands able to form metal complexes with particular characteristics is of great interest, and the characterization of ligand-metal interactions can be regarded as the first stage upon which to base new studies.

Among the different approaches that can be used in metal complex applications, one exploits the geometry imposed by the metal ion on the ligand, while another favours the synthesis of suitable ligands that are able to drive the metal ions in appropriate spatial positions.

Whatever the strategy followed, the ligand is very often designed to not saturate the

coordination requirement of the metal ion, meaning that the complex formed can fulfill its binding requirement by adding another species.[7-11]

Owing to the intriguing structural topologies of ligands, which lead to the formation of metal complexes, we recently synthesized receptors showing, or not, macrocyclic topologies containing phenol functions. These form mono and dinuclear complexes in which phenol or biphenol fragments play a fundamental role in both the stabilization of the metal ion and the photochemical response.[12-27]

Phenol and polyphenols have well known optical properties which mainly depend on their protonation degree.[28-31] In this study, we want to extend our knowledge of the spectroscopic properties of a ligand containing two 2,2'-biphenol moieties (BPH) that are linked to the ethylenediamine scaffold (**L** in Chart 1). In particular, our aim is to identify the ligand's possible application as both a chemosensor and a sequestrating agent for suitable metal ions.

Experimental part

General methods

UV absorption spectra were recorded at 298.1 K on a Varian Cary-100 spectrophotometer equipped with a temperature control unit. Fluorescence spectra were recorded at 298.1 K on a Varian Cary-Eclypse spectrofluorimeter and the spectra are uncorrected.

The fluorescence quantum yields were determined by comparing the integrated fluorescence spectra of the samples with 2,2'-biphenol in acetonitrile ($\Phi = 0.29$).[32]

^{1}H and ^{13}C NMR spectra were recorded at 298.1 K on a Bruker Avance instrument,

operating at 400.13 and 100.61 MHz, respectively.

Elemental analyses were performed with a Termofinnigan Flash 1112 EA CHN analyzer, mass spectra (MS-ESI) were acquired with a Waters Micromass ZQ mass spectrometer.

X-ray crystallography

Single crystal diffraction measurements for compounds [Ni(H_{-2}**L**)·2(*n*-BuOH)] (**4**), [Ni(H_{-2}**L**)·2(MeOH)] (**5**), [Cd(H_{-2}**L**)·2(DMF)] (**6**), [Cu(H_{-2}**L**)(DMF)] (**7**) and [Pd(H_{-2}**L**)(DMF)] (**8**) were carried out, at 150 K, with an Oxford Diffraction Excalibur diffractometer using the Mo-Kα radiation (λ = 0.71073 Å). Data collections were performed with the program CrysAlis CCD.[33] Data reductions were carried out with the program CrysAlis RED.[33] Finally, absorption corrections were performed with the program ABSPACK in CrysAlis RED.

The structures were solved by using the SIR-97 package[34] and subsequently refined on the F^2 values by the full-matrix least-squares program SHELXL-97.[35]

Geometrical calculations were performed by PARST97,[36] and molecular plots were produced by the programs ORTEP-3,[37] Mercury (v3.5)[38] and Discovery Studio Visualizer (v4.5).[39]

In all the structures the non-hydrogen atoms were refined anisotropically. In the nickel and palladium complexes the hydrogen atoms were found in the Fourier difference map; on the contrary, in the copper and in the cadmium species all the hydrogen atoms, except those bonded to O(2) and O(4) that were found in the Fourier difference map, were set in calculated positions and refined in agreement to the atoms to whom they are bonded. For the *n*-butanol molecule in **4**, as well as for the DMF one in **7**, two positions

were found and refined. In Table 1 crystal data and refinement parameters of the solid-state structures are reported.

Electromotive force (EMF) Measurements

Equilibrium constants for protonation and complexation reactions of the ligands were determined by pH-metric measurements (pH=−log[H^+]) in water/ethanol 50/50 v/v with 0.15 mol dm^{-3} NMe_4Cl at 298.1 ± 0.1 K, using the fully automatic equipment that has already described;[15] EMF data were acquired with the PASAT computer program.[40] The combined glass electrode was calibrated as a hydrogen concentration probe by titrating known amounts of HCl with CO_2-free NaOH solutions and determining the equivalent point by Gran's method,[41,42] which gives the standard potential $E°$ and the ionic product of water (pK_w = 14.48(1) at 298.1 K in water/ethanol 50/50 v/v with 0.15 mol dm^{-3} NMe_4Cl, $K_w = [H^+][OH^-]$). At least three potentiometric titrations were carried out for each system in the pH range 2-12, and all titrations were treated either as single sets or as separate entities, for each system; no significant variations were found in the values of the determined constants. The HYPERQUAD computer program was used to process the potentiometric data.[43]

Synthesis

All chemicals were purchased from Aldrich, Fluka and Lancaster in the highest quality commercially available. 3-bromomethyl-2,2'-dimethoxybiphenyl (**1**) was synthesized from 2,2'-biphenol as previous described.[44]

N,N'-Bis[(2,2'-dimethoxybiphen-3-yl)methyl]-N,N'-dimethylethylenediamine (3):

N,N'-dimethylethylenediamine (**2**) (0.5 cm^3, 404 mg, 4.6 mmol) and K_2CO_3 (10.2 g, 74 mmol) were suspended in refluxing DMF (100 cm^3). To this mixture, a solution of **1** (2.83 g, 9,2 mmol) in DMF (80 cm^3) was added dropwise over 1 h, after which the suspension was refluxed for 20 h and then filtered. The solution was poured in 1 dm^3 of ice/water mixture, the yellow solid phase was filtered and washed with cold water and dried obtaining 2,21 g of **3** (yield 89%). ^{1}H NMR ($CDCl_3$): 2.30 (s, 6H), 2.67 (s, 4H), 3.35 (s, 6H), 3.63 (s, 4H), 3.78 (s, 6H), 6.97-7.39 ppm (m, 14H), MS (ESI): m/z: 541 [$M+H^+$].

N,N'-Bis[(2,2'-dihydroxybiphen-3-yl)methyl]-N,N'-dimethylethylenediamine disodium salt monohydrate ($Na_2H_{-2}L\cdot H_2O$): Compound **3** (1.6 g, 3 mmol) and phenol (9.0 g, 96 mmol) were dissolved in HBr/CH_3COOH (33%, 80 cm^3). The solution was stirred at 90 °C for 22 h. The resulting suspension was filtered and washed with CH_2Cl_2 several times. The red solid obtained was dissolved in water (10 cm^3), filtered to eliminate the insoluble residues, and alkalinized to pH>12 by adding a 2 M NaOH solution. After 24 h the sodium salt Na_2H_{-2}**L** precipitates from the alkaline solution stored at 5 °C. The white solid was collected by vacuum filtration and washed with cold ethanol to obtain **L** (580 mg, 35%) as disodium salt Na_2H_{-2}**L**$\cdot H_2O$. ^{1}H NMR (D_2O, pH=11.5): 2.12 (s, 6H), 2.63 (s, 4H), 3.59 (s, 4H), 6.76 (m, 6H), 7.10 (m, 4H), 7.30 ppm (m, 4H); ^{1}3C NMR (D_2O): 41.2, 52.5, 55.2, 118.1, 118.2, 119.0, 125.6, 128.8, 129.1, 129.5, 130.3, 130.4, 131.0, 157.2, 159,1 ppm; analysis calcd for $C_{30}H_{32}N_2Na_2O_5$ (Na_2H_{-2}**L**$\cdot H_2O$, MM=546.57 g/mol): C 65.93, H 5.90, N 5.13; found: C 65.8, H 6.0, N 5.1, MM=547.8 g/mol.

[Ni(H_{-2}L)·2(*n*-BuOH)] (4): $Ni(ClO_4)_2·6H_2O$ (37 mg, 0.1 mmol) in acetonitrile (5 cm^3) was added to an acetonitrile solution (5 cm^3) containing Na_2H_{-2}**L**·H2O (55 mg, 0.1 mmol) and the solution was stirred at 80 °C for 1 hour. Butanol (0.5 cm^3) was added to the hot mixture, crystals suitable for X-ray analysis were obtained by slow evaporation (50 mg, 72%). Analysis calcd for $C_{38}H_{50}N_2NiO_6$ ([Ni(H_{-2}**L**)·2(*n*-BuOH)], MM=689.51 g/mol): C 66.19, H 5.90, N 4.06; found: C 66.0, H 6.1, N 4.0, MM=691.5 g/mol. MS (ESI): m/z: 541.1 $[NiH_{-1}L]^+$.

[Ni(H_{-2}L)·2(MeOH)] (5): $Ni(ClO_4)_2·6H_2O$ (37 mg, 0.025 mmol) in acetonitrile (5 cm^3) was added to an acetonitrile solution (5 cm^3) containing Na_2H_{-2}**L**·H_2O (55 mg, 0.1 mmol) and the solution was stirred at 80 °C for 1 hour. Methanol (0.5 cm^3) was added to the hot mixture, crystals suitable for X-ray analysis were obtained by slow evaporation. (41 mg, 68%). Analysis calcd for $C_{32}H_{38}N_2NiO_6$ ([Ni(H_{-2}**L**)·2(MeOH)], MM=605.35 g/mol): C 63.49, H 6.33, N 4.63; found: C 63.2, H 6.4, N 4.4, MM=608.2 g/mol. MS (ESI): m/z: 541.1 $[NiH_{-1}L]^+$

[Cd(H_{-2}L)·2(DMF)] (6): $Cd(ClO_4)_2·6H_2O$ (42 mg, 0.1 mmol) in acetonitrile (5 cm^3) was added to an acetonitrile solution (5 cm^3) containing Na_2H_{-2}**L**·H_2O (55 mg, 0.1 mmol) and the solution was stirred at 80 °C for 1 hour. DMF (0.5 cm^3) was added to the hot mixture, crystals suitable for X-ray analysis were obtained by slow evaporation. (58 mg, 78%). Analysis calcd for $C_{36}H_{44}CdN_4O_6$ ([Cd(H_{-2}**L**)·2(DMF)], MM=741.15 g/mol): C 58.34, H 5.98, N 7.56; found: C 58.2, H 6.1, N 7.4, MM=742.9 g/mol. MS (ESI): m/z: 597.1 $[CdH_{-1}L]^+$.

[Cu(H$_{-2}$L)(DMF)] (7): $Cu(ClO_4)_2 \cdot 6H_2O$ (37 mg, 0.1 mmol) in acetonitrile (5 cm^3) was added to an acetonitrile solution (5 cm^3) containing $Na_2H_{-2}\mathbf{L}\cdot H_2O$ (55 mg, 0.1 mmol) and the solution was stirred at 80 °C for 1 hour. DMF (0.5 cm^3) was added to the hot mixture, crystals suitable for X-ray analysis were obtained by slow evaporation. (47 mg, 75%). Analysis calcd for $C_{33}H_{37}N_3CuO_5$ ([Cu(H$_{-2}$**L**)(DMF)], MM=619.19 g/mol): C 64.01, H 6.02, N 6.79; found: C 63.8, H 6.2, N 6.7, MM=621.3 g/mol. MS (ESI): m/z: 546.2 $[CuH_{-1}\mathbf{L}]^+$.

[Pd(H$_{-2}$L)(DMF)] (8): K_2PdCl_4 (33 mg, 0.1 mmol) in DMF (5 cm^3) was added to a DMF solution (5 cm^3) containing $Na_2H_{-2}\mathbf{L}\cdot H_2O$ (55 mg, 0.1 mmol) and the solution was stirred a 80 °C for 4 hour. Crystals suitable for X-ray analysis were obtained by slow evaporation. (46 mg, 70%). Analysis calcd for $C_{33}H_{37}N_3PdO_5$ ([Pd(H$_{-2}$**L**)(DMF)], MM=662.05 g/mol): C 59.87, H 5.63, N 6.35; found: C 59.8, H 5.8, N 6.2, MM=662.8 g/mol. MS (ESI): m/z: 589.1 $[PdH_{-1}\mathbf{L}]^+$.

Caution. *Perchlorate salts of organic compounds are potentially explosive; these compounds must be prepared and handled with care!*

Results and discussion

Synthesis

The synthetic pathway used to obtain **L** is depicted in Scheme 1. The reagent 3-bromomethyl-2,2'-dimethoxybiphenyl (**1**) was synthesized starting from 1,1'-biphenol,

while the hydroxyl functions were protected with the methyl group, as previously reported.[44] The protected ligand (**3**) was obtained in high yield by reacting two equivalents of **1** with N,N'-dimethylethylenediamine (**2**) in DMF in the presence of K_2CO_3 as a base. The demethylation of the phenolic oxygen atoms was carried out with a 33% HBr solution in glacial acetic acid in the presence of phenol. **L** was purified as a $Na_2H_{-2}\mathbf{L}\cdot H_2O$ salt by crystallization from a NaOH solution (see the experimental part). The Ni(II), Cu(II), Cu(II) and Pd(II) complexes with **L** were synthesized and characterized both in solution and solid state. Solid complexes **4**, **5**, **6** and **7** have been obtained in high yield by mixing the $Na_2H_{-2}\mathbf{L}$ species and the corresponding perchlorate salt, namely $Ni(ClO_4)_2\cdot 6H_2O$, $Cu(ClO_4)_2\cdot 6H_2O$ or $Cd(ClO_4)_2\cdot 6H_2O$, in acetonitrile solution containing a co-solvent as butanol, methanol or DMF and refluxing the mixture for 4 hour. Pd(II) complex (**8**) was synthesized by adding K_2PdCl_4 to a solution of $Na_2H_{-2}\mathbf{L}$ in DMF at 80°C, DMF was used as solvent due to the insolubility of K_2PdCl_4 in acetonitrile. Metal complexes, precipitated from the cold solution, were characterized by elemental analysis, mass spectroscopy and single crystal X-ray diffractometry. The compounds resulted neutral complexes of formula $[MH_{-2}\mathbf{L}]$ with one or two molecules of solvent coordinated to the metal ion.

X-ray solid state structures

In the asymmetric units of **4** and **5** one half of the metal complex is present, being the two halves of the metal complex related by one symmetry axis: −x+1, y, −z+1/2 and −x, y, −z+3/2 for **4** and **5**, respectively. In the other investigated compounds, the asymmetric unit consisted of one metal complex.

The $H_{-2}\mathbf{L}^{2-}$ anion provided four donor atoms in all the metal complexes: two nitrogen

atoms from the polyamine moiety and two oxygen atoms from the BPH units. While these donors sufficed when it came to saturating the coordination sphere of the palladium ion, the other metal cations completed their coordination spheres with donor atoms provided by the solvent molecules, i.e. the oxygen atoms of two alcohol molecules in the nickel complexes (*n*-butanol and methanol in **4** and **5**, respectively), and the oxygen atoms provided by two and one DMF molecules in the cadmium (**6**) and copper (**7**) complexes, respectively (see figures 1-5).

Bond distances and angles of the coordination spheres, which were within the expected ranges, are reported in Table 2.

The nickel complexes (**4** and **5**) were, as expected, almost identical (Figure 6a), while the overall shape of the cadmium complex in **6** differed essentially from the previous ones in terms of the orientations of the BPH moieties, as evidenced in Figure 6(b). In fact, as reported in Table 3, while the conformation of the ethylenediamine unit of $[H_{-2}\mathbf{L}]^{2-}$, as defined by the dihedral angles τ3, τ4 and τ5, was the same in the nickel and cadmium complexes, the dihedral angles defining the arrangement of the BPH side arms (τ1, τ2, τ6 and τ7) were definitely different in the latter. Finally, the $[MH_{-2}\mathbf{L}]$ moieties in **7** and **8** (Figure 6c) were well superimposable.

In compounds **4**, **5** and **6**, the metal cation was hexacoordinated and the coordination polyhedron was well described by an octahedron. The coordination environment of the copper cation in **7** was square pyramidal (sp) [τ index = 0.003],[45] while in **8** the tetracoordinated Pd(II) ion showed, as expected, the usual square planar disposition of the donor atoms. Interestingly, the Pd(II) cation was 3.657(3) Å apart from the oxygen atom of one DMF molecule [O(1d)], and the line passing through Pd(1)-O(1d) formed an angle of 86.31(6)°, with the mean plane defined by the four donor atoms N(1), N(2),

O(1) and O(3). The relative orientation of the [PdH_{-2}**L**] complex and the DMF molecule may suggest the existence of a weak bonding interaction between the metal centre and the oxygen atom of DMF, although the Pd(1)···O(1d) distance is somewhat long. This is consistent with a [4+1] coordination. [46] Finally a net of weak hydrogen bonds between the DMF molecule and the [PdH_{-2}**L**] complex is present (see table S1); such net connects together two symmetry related complexes.

Meanwhile, the $[H_{-2}\mathbf{L}]^{2-}$ ligand around the metal cation adopted a trans conformation[10] in **7** and **8**, and, due to the presence of two asymmetric nitrogen atoms in the complex, gave rise to an [R,S] and [R,R]/[S,S] trans topology in the copper and palladium complexes, respectively (Figure 7).[10]

It is interesting to note that a survey in the Cambridge Structural Database[47] (CSD, v 5.37) shows that, in complexes of ligands similar to $H_{-2}\mathbf{L}^{2-}$, with a *trans* conformation around the metal cation, the [R,R] / [S,S] configuration of the two asymmetric nitrogen atoms is not the preferred one; in fact, such a configuration is present in just 20 fragments out of 67 (found in 51 hits), with the preferred one being the [R,S].

Finally, in the nickel and cadmium complexes, the usual [R,R]/[S,S] cis-α[48] topology was observed (Figure 7). Incidentally, such a topology is adopted by all the 43 hexacoordinated complexes with ligands similar to $H_{-2}\mathbf{L}^{2-}$ found in the CSD.

As for the crystal packing, there were no relevant intermolecular interactions present in **6**, **7** and **8**, with the only strong hydrogen bonds[49] being those found in the five complexes involving the hydroxyl/hydroxylate belonging to the same BPH arm (see Table 4).

In **4** and **5**, on the other hand, the *n*-butanol molecule bridged two nickel complexes, giving rise to ribbons that were perpendicular to the b axis in **4** and propagating along

the c axis in **5** (Table 4 and figures S1 and S2).

Acid-base behaviour

Potentiometric measurements

Table 5 summarizes the basicity constants of **L**, which were potentiometrically determined in a 0.15 mol dm^{-3} NMe_4Cl ethanol/water 50/50 v/v solution at 298.1 K. The mixed solvent was used to increase the solubility of the **L** species around pH=7 in an aqueous solution. The neutral form of **L** can potentially add two protons as well as dissociate four protons. However, under the experimental conditions used, it behaved as a diprotic base and a diprotic acid. Taking into account the fact that the total number of **L** sites that can be involved in the acid-base processes is six (two nitrogen and four oxygen atoms), the acid−base behavior of **L** was somewhat unexpected, given that only four of the sites were directly involved in our experimental conditions. As shown in Table 5, **L** can be present in an alkaline solution such as a $H_{-2}\mathbf{L}^{2-}$ species. Analyzing the protonation constants starting from this anionic species, it was found that $H_{-2}\mathbf{L}^{2-}$ behaved as a rather strong base in the first protonation step (log$K$=10.92), meaning that this stage probably mainly involves one of the two tertiary amine functions. The protonation constant of the species $H_{-1}\mathbf{L}^{-}$ was log$K$=8.00 and, for the next two protonation steps, the basicity was somewhat regularly reduced by approximately two log units for each protonation step, as expected from the increase in the positive charge's repulsion as the molecule becomes more protonated. The final two acidic protons on the $H_{-2}\mathbf{L}^{2-}$ species could not be removed under our experimental conditions, suggesting the presence of a strong hydrogen-bonding network to stabilize them in the molecule, as

reported in our previous papers on ligands containing the 2,2'-biphenol fragment.[22] Interestingly, such strong interactions were still present in the solid-state crystal structures reported here; in fact, it was observed that strong hydrogen bonds involving hydroxyl/hydroxylate groups belonging to the same BPH arm were present in all the five complexes (Table 4).

UV-Vis, fluorescence and NMR studies.

UV/Vis absorption electronic spectra of **L** were obtained in an ethanol/water (50/50 v/v) solvent at different pH values in order to determine the role of the phenolic functions in the acid-base behaviour of **L**. The spectra showed different wavelength maxima (λ_{max}) depending on the pH. At pH=2, where the $H_2\mathbf{L}^{2+}$ species was prevalent in the solution, the spectrum exhibited a main band with λ_{max}=284 nm (ε=14600 cm^{-1} mol^{-1} dm^3), while at pH=12, where the $H_{-2}\mathbf{L}^{2-}$ species prevailed in the solution, the spectrum exhibited a band with λ_{max}=313 nm (ε=16700 cm^{-1} mol^{-1} dm^3) (Figure S3). These differences were due to the deprotonation of the phenolic groups occurring at high pH values. The change in λ_{max} was ascribed to the presence of the hydroxyl phenol form at low pH levels and to the phenolate form at high pH values. It was possible to determine the step during which the BPH moieties were involved in the deprotonation processes by plotting the absorbance of the spectra at λ=313 nm as a function of pH and coupling this with the distribution diagram of the species obtained by potentiometric measurements (Figure 8). The absorbance was approximately zero for pH<5, but it started to increase at higher pH values, reaching its maximum and remaining constant for pH≥9. As shown in Figure 8, the absorbance started to increase with the appearance of the neutral **L** species. It then continued to rise with the appearance of the $H_{-1}\mathbf{L}^{-}$ species in solution,

before reaching a plateau for pH≥9, where the latter species was fully formed. Taking into account the fact that the change in absorbance was due to the deprotonation of the phenol groups, the profile can be attributed to a first deprotonation of the chromophores occurring in the **L** species and to a second deprotonation in the $H_{-1}\mathbf{L}^{-}$ species. In fact, when the **L** species was prevalent in the solution, the molar absorptivity (ε) at 313 nm was about 8000 cm^{-1} mol^{-1} dm^3, and this value doubled when the $H_{-1}\mathbf{L}^{-}$ species prevailed in the solution. This means that the neutral **L** species was amphionic under the experimental conditions. Upon the addition of an excess of NMe_4OH, no further changes were observed in the absorption spectra, suggesting that no further deprotonation processes occurred in the BPH arms, even at strongly alkaline pH values.

These data can be merged with those obtained by ^{1}H-NMR experiments performed at different pH values in a CD_3OD/D_2O 50/50 v/v mixed solvent, which furnished more information about the localization of the acidic protons in the protonated species; ^{1}H-^{1}H and ^{1}H-^{13}C NMR correlation experiments were performed to assign all the signals. The trend in chemical shifts of the most significant resonances, reported as a function of pH, is shown in Figure 9. The ^{1}H-NMR spectrum recorded at pH=2, where $H_2\mathbf{L}^{2+}$ was prevalent in the solution, exhibited a singlet at δ=2.81 ppm, integrating six protons attributed to the resonances of the protons H11 (H11, 6H), a broad singlet at δ=3.58 ppm (H12, 4H), another broad singlet at 4.30 ppm (H10, 4H), and the aromatic signals integrating for 14 H from 6.84 to 7.17 ppm (Figure S4). In particular, we followed the behaviour of the H8 aromatic proton belonging to the rings that were linked close to the diamine scaffold and were in a *para*-position to the OH group; H8 produced a triplet at δ=6.93 ppm (H8, 2H). The spectral feature indicated a C_{2v}-symmetry mediated on the NMR time-scale, which was preserved throughout the pH range investigated.

At the lowest pH values, where the fully protonated species $H_2\mathbf{L}^{2+}$ was present in the solution, the two amine functions were protonated, as were the BPH groups (Scheme 2). By increasing the pH to the value at which the $H\mathbf{L}^{+}$ species was prevalent in the solution (pH=5.5), all the signals underwent an upfield shift, with the aliphatic protons (H10, H11 and H12) undergoing the highest shift, suggesting that the first deprotonation step mainly involved a tertiary amine function in accordance with the UV-Vis measurements. At pH=7.2, where the neutral **L** species was prevalent in the solution, many of the resonance signals shifted. In particular, the resonance of the aromatic proton H8 showed a marked upfield shift (Figure 9), suggesting that this deprotonation step mainly involves one of the two BPH groups and, in particular, the phenol group close to the amine scaffold. This hypothesis is in agreement with the UV/Vis measurements, which indicated the involvement of the BPH chromophores in the deprotonation step going from $H\mathbf{L}^{+}$ to **L**. H8 underwent a further upfield shift to pH=9.00, where the $H_{-1}\mathbf{L}^{-}$ species was prevalent in the solution (Figure 9), suggesting that this deprotonation step occurs on the other BPH group. Looking at the UV/Vis spectra in this pH-range, the absorbance at 316 nm doubled in value, confirming the deprotonation of a second phenol group close to the amine moiety. The final deprotonation step involved the amine function; in fact, only the protons H10, H11 and H12, but not H8, underwent a marked up-field shift, going from pH=9 to pH=12.

The fluorescence spectra of **L** at various pH-values were acquired to determine the emissive behaviour of the protonated forms of **L**. These spectra were registered by excitation at the isosbestic point of the UV-Vis spectra (λ_{ex}=290 nm) (Figure S3). When examining the trend of the emission intensity at 401 nm, as reported in Figure 8, it is evident that the $H_2\mathbf{L}^{2+}$ and $H\mathbf{L}^{+}$ are not fluorescent, while the strongly emissive species

are the $H_{-1}\mathbf{L}^{-}$ and $H_{-2}\mathbf{L}^{2-}$ versions. Taking into account the fact that, as reported in our previous papers, the 2,2'-biphenol moiety is highly fluorescent only in its deprotonated form,[25] this trend confirms the protonation reported in Scheme 2. The intensity of the fluorescence emission of the ligand was highly dependent on the protonation state of the BPH groups, however the shape and the λ_{em} of the spectra were independent on pH, meaning that the overall emission was only due to the monoanionic excited state of BPH groups. It is interesting to note that the emission behaviour of **L** was not PET-mediated; in fact, the emission intensity was not dependent on the protonation state of the amine functions. To confirm this hypothesis, quantum yield measurements of free BPH and **L** were taken in an ethanol/water solution at pH=12, producing $\Phi_{biphenol}$=0.69±0.05 and $\Phi_{H-2\mathbf{L}}$=0.70±0.05 and demonstrating that the quantum yield of the deprotonated BPH groups was not perturbed by the diamine scaffold. The neutral **L** species, in which only one BPH group was deprotonated, was weakly fluorescent and its fluorescence quantum yield ($\Phi_{\mathbf{L}}$=0.07±0.02) was less than half of those of the $H_{-1}\mathbf{L}^{-}$ species in which both BPH arms were deprotonated ($\Phi_{H-1\mathbf{L}}$=0.60±0.05). This means that the intramolecular excited state proton transfer (ESPT) from the protonated to the deprotonated BPH moieties quenched the fluorescence emission.[50-52] Plotting the calculated quantum yield, obtained multiplying the quantum yield of the single protonated species of **L** by their molar fraction (Equation S1), as a function of pH a perfect accordance with the trend of emission intensity was obtained (see Figure 8).

Metal ion complexation

The coordination behaviour of **L** towards the Ni(II), Cu(II) and Zn(II) metal ions was studied by potentiometry and UV-Vis and fluorescence spectrophotometry, while the

interaction with the Cd(II) and Pd(II) ions was examined by UV-Vis and fluorescence spectrophotometry only, because their complexes precipitated in the EMF experimental conditions.

Potentiometric studies

Table 6 reports the stability constants of **L**, with Ni(II), Cu(II) and Zn(II) metal ions measured at 298.1 K in an 0.1 M NMe_4Cl EtOH/aqueous 50/50 v/v solution. **L** formed mononuclear complexes with Ni(II) and Zn(II), and both mono- and dinuclear complexes with the Cu(II) ion in the solution. As expected, the Cu(II) species had higher stability constants than those of the Ni(II) and Zn(II) metal ions, and the trend of the formation constants was Cu(II)>Ni(II)>Zn(II), following the Irwing-Williams series. All three metal ions formed highly stable metal complexes with $[MH_{-2}\mathbf{L}]$ stoichiometry, with formation constants of log$K$=18.55, 14.42 and 12.06 for Cu(II), Ni(II) and Zn(II), respectively (Table 6). All the metal complexes were able to add one or two protons, probably by the phenolate groups, giving rise to $[ZnH_{-1}\mathbf{L}]^{+}$, $[CuH_{-1}\mathbf{L}]^{+}$ and $[Ni\mathbf{L}]^{2+}$species. In the mononuclear Cu(II) complex, one proton could be removed from the $[CuH_{-2}\mathbf{L}]$ species, with a log$K$=−12.35 giving rise to the $[CuH_{-3}\mathbf{L}]^{-}$ species. This occurred in the BPH moiety, as clearly highlighted by the UV-Vis experiments (see the next section).

In the Cu(II)/**L** system, a stable dinuclear species with $[Cu_2H_{-2}\mathbf{L}]^{2+}$ stoichiometry was also found. Probably, both the OH groups of each BPH arm in this species were involved in the coordination of the metal ions, strongly increasing the acidity of the two phenol rings. In fact, the $[Cu_2H_{-2}\mathbf{L}]^{2+}$ species easily lost two protons, giving rise to the dinuclear species $[Cu_2H_{-3}\mathbf{L}]^{+}$ and $[Cu_2H_{-4}\mathbf{L}]$, one of which had a log$K$ of −5.12 and

−10.49 for the first and second deprotonation steps, respectively. Finally, the neutral $[Cu_2H_{-4}\mathbf{L}]$ species was able to add one or two OH^- anions, giving rise to the hydroxylated $[Cu_2H_{-4}\mathbf{L}OH]^-$ and $[Cu_2H_{-4}\mathbf{L}(OH)_2]^{2-}$ species, with addition constants of log*K*=3.54 and 2.65 for the first and second OH^- additions, respectively. These values led us to suppose that the OH^- were not bound by the bridge disposition between the two Cu(II) ions, meaning that these two ions do not cooperate in binding the anions.[53]

UV-Vis and fluorescence studies

In order to understand the role of the BPH groups in the metal ion coordination, the UV-Vis absorption and fluorescence spectra of **L** in the presence of increasing amounts of transition metal ions were recorded in an ethanol/water (50/50 v/v) solvent at buffered pH=7.4 (HEPES). In these experimental conditions, **L** showed two absorption bands at λ_{max}=286 and 313 nm that were assigned to the protonated and deprotonated forms of the 2,2'-biphenol, respectively, as discussed above (Scheme 2 and Figure S3). By adding metal ions, the absorption and emission spectra underwent radical changes depending on the metal ion investigated, but in general the band of the protonated form at 286 nm decreased in intensity and a new band at a lower energy appeared, denoting the involvement of BPH groups in the metal ion coordination.

Addition of Ni(II), Zn(II) and Cd(II). The addition of Ni(II), Zn(II) or Cd(II) metal ions to a solution of **L** in 50/50 v/v ethanol/aqueous HEPES (pH=7.4) caused the disappearance of the band at 286 nm and the appearance of a band near 313 nm, resulting in a blue-shift with respect to the corresponding band in the pure deprotonated form (Figure 10). This is in agreement with the deprotonation of the phenol moiety that

occurred when the complexes formed (see X-ray solid state structures) (Figure 11). Analyzing the fluorescent emission, the addition of Zn(II) and Cd(II) switched on the emission at 401 nm ($\Phi_{ZnH_{-2}\mathbf{L}}$=0.68±0.05 and $\Phi_{CdH_{-2}\mathbf{L}}$=0.53±0.05), and also exhibited a slightly blue shift of the emission wavelength (Figure 10). The increase of the emission band can mainly be ascribed to the stabilization of the deprotonated form of the BPH groups in the mononuclear species at pH=7.4 (Figure 11). In the case of the Zn(II)/**L** system, it was possible to merge the emission with the distribution diagram of the species as a function of pH (Figure 11 d). The figure highlights that the [ZnH_{-2}**L**] was the highest emitting species. Similar trend of the emission as a function of pH was obtained for the Cd(II)/**L** system (data not reported). In contrast, the addition of Ni(II) quenched the fluorescence emission, probably due to the paramagnetic effect (Figure 10). It is noteworthy that, in this system, the fluorescence responses to Zn(II) and Cd(II) could not be ascribed to the suppression of PET, as observed in most Zn(II) sensors,[25,54-56] but instead depended on the stabilization of the dianionic form of **L** upon metal complexation.

Addition of Cu(II). As reported by the EMF studies, **L** is able to form mono and dinuclear Cu(II) complexes (Figure 11, Table 6). The titration of a solution of **L** in ethanol/aqueous HEPES pH=7.4 50/50 v/v with Cu(II) (from a 0 to 1 equivalent) resulted in the increase of the band at 302 nm. This suggested the deprotonation of the OH group of both BPH moieties close to the amine functions due to the formation of the [CuH_{-2}**L**] species (see X-ray solid state structures). A band also appeared at 410 nm that was attributable to the LMCT transition from one phenolate oxygen to the Cu(II) cation (Figure 12).[57-59] In the presence of two equivalents of Cu(II), the [Cu_2H_{-4}**L**] species

formed and the ligand band at 302 nm moved to 288 nm, indicating the deprotonation of the second OH group of each BPH. Meanwhile, the LMCT band at 410 nm moved to 383 nm, suggesting the involvement of both the oxygen atoms of each fully deprotonated BPH moiety in the coordination of the second metal ion.[59] Based on the potentiometric and UV-Vis data, we speculate that the first Cu(II) ion in the dinuclear $[Cu_2H_{-4}\mathbf{L}]$ complex is coordinated by the two amine groups and the two deprotonated phenol oxygen atoms close to the diamine scaffold. Meanwhile, the second Cu(II) ion is probably stabilized by the four oxygen atoms of the converging BPH moieties. In this way, the deprotonated oxygen atom of the two phenols close to the diamine fragment bridges the two Cu(II) ions.

As expected, the addition of Cu(II) quenched the fluorescence emission, mainly due to paramagnetic effect. In particular, the addition of the first and second Cu(II) ions quenched 92% and 100% of the emissions at 400 nm, respectively (Figure 12).

Addition of Pd(II). The addition of one equivalent of a Pd(II) ion such as K_2PdCl_4 to a solution of **L** in an ethanol/aqueous HEPES (pH=7.4) 50/50 v/v mixture caused the appearance of the band at 303 nm that is attributable to the coordinated and deprotonated form of BPH involved in the $[PdH_{-2}\mathbf{L}]$ complex. The trend is quite similar to that observed for the addition of one equivalent of Cu(II), suggesting a similar coordination environment for both metal ions, as supported by the X-ray diffraction data (Figure 6). No changes in the absorption band were observed upon the addition of further Pd(II) equivalents, and so we can exclude the formation of dinuclear species. As confirmed by the solid state structure, in the mononuclear complex, the Pd(II) saturated all its coordination sites in a stable square planar geometry. The Pd(II) complex was not

fluorescent (Figure 12) due to the heavy-atom effect that promotes the intersystem-crossing of the excited state, as observed for several square planar Pd(II) complexes with strong π-donating ligands.[60]

Concluding remarks

The synthesis, acid-base and coordination studies of the new ligand N,N'-Bis[(2,2'-dihydroxybiphen-3-yl)methyl]-N,N'-dimethylethylenediamine (**L**) are reported herein, as are the solid-state structures of its Ni(II), Cd(II), Cu(II) and Pd(II) metal complexes. **L** behaves as a diprotic base, and diprotic acid in an ethanol/water 50/50 v/v solution and its emission properties strongly depend on the protonation degree of the BPH moieties. In fact, **L** is not fluorescent when both BPH groups are protonated (pH<6), while it shows a strong emission band at 408 nm when both of these groups are in the anionic form (pH>10). Interestingly, the emission of this system is not PET-mediated, and the deprotonation of both BPH arms is needed to achieve the highest fluorescence quantum yield. The $H_{-2}\mathbf{L}^{2-}$ species provides, in principle, six donor atoms, i.e. the two nitrogen atoms bearing the ethylenediamine moiety and the four oxygen atoms of the BPH units. The flexibility of **L** makes it able to coordinate metal ions, with different coordination requirements losing selectivity; in fact, it is able to form mononuclear metal complexes with transition metal ions such as Ni(II), Cu(II), Zn(II), Cd(II) and Pd(II). In all these species, the metal ion is stabilized by only four donor atoms, namely the two nitrogen and two oxygen atoms of the phenolate units close to the diamine scaffold. While these donors are enough to fulfill the coordination requirement of the Pd(II) ion, the other metal cations investigated, e.g. Ni(II), Cu(II), Zn(II) and Cd(II),

remain unsaturated and are prone to bind both other species-like anions such as OH^- in solution and neutral molecules, as highlighted by the solid state crystal structures. Furthermore, both mononuclear and dinuclear Cu(II) metal complexes are able to bind anionic and neutral species, as in the [Cu(H_{-2}**L**)(DMF)] (**7**) complex, in order to complete the coordination requirement of the metal ion. The presence of two BPH moieties allows us to study the metal-ligand interaction via spectrophotometric experiments, because their involvement in the coordination of the metal ions results in radical changes in the absorption and emission spectra. The main finding of this study is that **L** responds (switching on the fluorescent emission) to the presence of Zn(II) and Cd(II) at pH=7.4, while the other metal ions completely quench the ligand. Accordingly, **L** can behave as a fluorescent chemosensor for metal ions.

In conclusion, the ligand **L** is able to bind transition metal ions in a water/ethanol mixture, giving rise to a spectrophotometric and spectrofluorimetric response depending on the pH of the solution. Coordination and photochemical properties, coupled with easy synthesis, indicate that **L** is an interesting building block with which to develop further sensors or metallo-receptors that link it to other coordinating active scaffolds, polymers, dendrimers or nanoparticles.

Acknowledgments

We would like to acknowledge the financial support provided by the Department of Pure and Applied Sciences at the University of Urbino and CRIST (Centro di Cristallografia Strutturale – University of Florence), where the X-ray diffraction data were collected.

Supporting information

X-ray crystallographic data of [Ni(H_{-2}**L**)·(*n*-BuOH)] (**4**), [Ni(H_{-2}**L**)·2(MeOH)] (**5**), [Cd(H_{-2}**L**)·2(DMF)] (**6**), [Cu(H_{-2}**L**)(DMF)] (**7**) and [Pd(H_{-2}**L**)(DMF)] (**8**) in CIF format, crystal packing of [Ni(H_{-2}**L**)·2(n-BuOH)] (**4**) and [Ni(H_{-2}**L**)·2(MeOH)] (**5**), UV-vis, fluorescence and ^{1}H-NMR acid-base titration of **L** from pH=2 to 12, and the mathematical model of the fluorescence quantum yield of **L** as a function of pH are available as Supporting Information.

References

(1) Lusby, P. J. *Annu. Rep. Prog. Chem., Sect. A: Inorg. Chem.* **2013**, *109*, 254−276.

(2) Roat-Malone, M. *Bioinorganic Chemistry: A Short Course*, 2nd Edition Rosette ISBN: 978-0-471-76113-6 October 2007 Wiley.

(3) Fanelli, M.; Formica, M.; Fusi, V.; Giorgi, L.; Micheloni, M.; Paoli, P. *Coord. Chem. Rev.* **2016**, *310*, 41−79.

(4) Jones, C. J.; Thornback, J. R. *Medicinal applications of coordination chemistry*. RSC, Cambridge, 2009.

(5) Gheorghe, D. Homogeneous Catalysis with Metal Complexes. Springer Series in Chemical Physics, 2012. ISBN: 978-3-642-24628-9.

(6) Formica, M.; Fusi, V.; Giorgi, L.; Micheloni, M. *Coord. Chem. Rev.* **2012**, *256*, 170−192.

(7) Ambrosi, G.; Formica, M.; Fusi, V.; Giorgi, L.; Micheloni, M. *Coord. Chem. Rev.* **2008**, *252*, 1121-1152.

(8) Ambrosi, G.; Formica, M.; Fusi, V.; Giorgi, L.; Guerri, A.; Micheloni, M.; Paoli, P.; Pontellini, R.; Rossi, P. *Inorg. Chem.* **2007**, *46*, 309−320.

(9) Benelli, C.; Borgogelli, E.; Formica, M.; Fusi, V.; Giorgi, L.; Macedi, E.; Micheloni, M.; Paoli, P.; Rossi, P. *Dalton. Trans.* **2013**, *42*, 5848-5859

(10) Amatori, S.; Ambrosi, G.; Fanelli, M.; Formica, M.; Fusi, V.; Giorgi, L.; Macedi, E.; Micheloni, M.; Paoli, P.; Rossi, *P. Chem. Eur. J.* **2014**, *20*, 11048−11057.

(11) Ambrosi, G.; Formica, M.; Fusi, V.; Giorgi, L.; Guerri, A.; Micheloni, M.; Paoli, P.; Pontellini, R.; Rossi, P. *Chem. Eur. J.* **2007**, *13*, 702−712.

(12) Berti, E.; Caneschi, A.; Daiguebonne, C.; Dapporto, P.; Formica, M.; Fusi, V.; Giorgi, L.; Guerri, A.; Micheloni, M.; Paoli, P.; Pontellini, R.; Rossi, P. *Inorg. Chem.* **2003**, *42*, 348−357.

(13) Ambrosi, G.; Formica, M.; Fusi, V.; Giorgi, L.; Guerri, A.; Micheloni, M.; Paoli, P.; Pontellini, R.; Rossi, P. *Inorg. Chim. Acta* **2003**, *356*, 203−209.

(14) Ambrosi, G.; Dapporto, P.; Formica, M.; Fusi, V.; Giorgi, L.; Guerri, A.; Micheloni, M.; Paoli, P.; Rossi, P. *J. Supramol. Chem.* **2002**, *2*, 301−303.

(15) Dapporto, P.; Formica, M.; Fusi, V.; Micheloni, M.; Paoli, P.; Pontellini, R.; Rossi, P. *Inorg. Chem.* **2000**, *39*, 4663−4665.

(16) Dapporto, P.; Formica, M.; Fusi, V.; Giorgi, L.; Micheloni, M.; Paoli, P.;

Pontellini, R.; Rossi, P. *Inorg. Chem.* **2001**, *40*, 6186−6192.

(17) Ceccanti, N.; Formica, M.; Fusi, V.; Giorgi, L.; Micheloni, M.; Pardini, R.; Pontellini, R.; Tiné, M. R. *Inorg. Chim. Acta* **2001**, *321*, 153-161.

(18) Formica, M.; Giorgi, L.; Fusi, V.; Micheloni, M.; Pontellini, R. *Polyhedron* **2002**, 21, 1351-1356.

(19) Fusi, V.; Llobet, A.; Mahia, J.; Micheloni, M.; Paoli, P.; Ribas, X.; Rossi, P. *Eur. J. Inorg. Chem.* **2002**, 4, 987−990.

(20) Dapporto, P.; Formica, M.; Fusi, V.; Micheloni, M.; Paoli, P.; Pontellini, R.; Romani, P.; Rossi, P. *Inorg. Chem.* **2000**, *39*, 2156−2163.

(21) Aguilar, J. A.; Descalzo, A. B.; Diaz, P.; Fusi, V.; Garcia-España, E.; Luis, S. V.; Micheloni, M.; Ramirez, J. A.; Romani, P.; Soriano, C. *J. Chem. Soc. Perkin Trans.* **2000**, 2, 1187−1192.

(22) Ambrosi, G.; Dapporto, P.; Formica, M.; Fusi, V.; Giorgi, L.; Guerri, A.; Micheloni, M.; Paoli, P.; Pontellini, R.; Rossi, P. *Chem. Eur. J.* **2003**, 9, 800−810.

(23) Ambrosi, G.; Formica, M.; Fusi, V.; Giorgi, L.; Guerri, A.; Micheloni, M.; Pontellini, R.; Rossi, P. *Polyhedron* **2003**, 22 (8), 1135−1146.

(24) Dapporto, P.; Formica, M.; Fusi, V.; Micheloni, M.; Paoli, P.; Pontellini, R.; Rossi, P. *Supramol. Chem.* **2001**, *13*, 369−377.

(25) Ambrosi, G.; Battelli, C.; Formica, M.; Fusi, V.; Giorgi, L.; Macedi, E.; Micheloni, M.; Pontellini, R; Prodi, L. *New J. Chem*. **2009**, *32*, 1−10.

(26) Ambrosi, G.; Formica, M.; Fusi, V.; Giorgi, L.; Guerri, A.; Macedi, E.; Micheloni, M.; Paoli, P.; Pontellini, R; Rossi, P. *Inorg. Chem*. **2009**, *48*, 5901−5912.

(27) Ambrosi, G.; Formica, M.; Fusi, V.; Giorgi, L.; Macedi, E.; Micheloni, M.; Paoli, P.; Rossi, P. *Inorg. Chem*. **2009**, *48*, 10424−10434.

(28) Bridges, J. W.; Creaven, P. J.; Wiliams, R. T. *Biochem. J.* **1965**, *96*, 872−878.

(29) Mohanty, J.; Pal H.; Sapre, A. V.; *Bull. Chem. Soc. Jpn.*, **1999**, *72*, 2193−2202.

(30) Feitelson, J. *J. Phys. Chem.*, **1964**, 68, 391−397.

(31) Krauss, M. J.; Jensen, O.; Hameka, H. F.; *J. Phys. Chem.* **1994**, 9955−9959.

(32) Jyotirmayee, M.; Pal H.; Sapre, A. V. *Bull. Chem. Soc. Jpn.* **1999**, 72, 2193.

(33) CrysAlisPro, Agilent Technologies, 2011.

(34) Altomare, A.; Cascarano, G. L.; Giacovazzo, C.; Guagliardi, A.; Moliterni, A.G.; Burla, M. C.; Polidori, G.; Camalli, M., Spagna, R., *J. Appl. Cryst.*, **1999**, *32*, 115−119.

(35) Sheldrick, G. M. SHELX 97, University of Göttingen, Germany, 1997.

(36)Nardelli, M. *J. Appl. Cryst*. **1995**, *28*, 659.

(37) Farrugia, L. J. *J. Appl. Cryst.* **1997**, 30, 565.

(38) Macrae, C.F.; Bruno, I.J.; Chisholm, J.A.; Edgington, P.R.; McCabe, P.; Pidcock, E.; Rodriguez-Monge, L.; Taylor, R.; van de Streek, J.; Wood, P.A. *J. Appl. Cryst.* **2008**, *41*, 466-470.

(39) Dassault Systèmes BIOVIA, Discovery Studio Visualizer, Release 4.5, San Diego: Dassault Systèmes, 2015.

(40) Fontanelli, M.; Micheloni, M. I Spanish–Italian Congress, Thermodynamics of Metal Complexes, PeÇiscola, 1990, University of Valencia Spain.

(41) Gran, G. *Analyst* **1952**, *77*, 661−671.

(42) Rossotti, F. J.; Rossotti, H. *J. Chem. Educ.* **1965**, *42*, 375.

(43) Gans, P.; Sabatini, A.; Vacca, A.; *Talanta* **1996**, *43*, 1739−1753.

(44) Ambrosi, G.; Dapporto, P.; Formica, M.; Fusi, V.; Giorgi, L.; Guerri, A.; Micheloni, M.; Paoli, P.; Pontellini, R.; Rossi, P. *Chem. Eur. J.* **2003**, 9, 800−810.

(45) Karunakan, C.; Thomas, K. R. J.; Shunmugasundaram, A.; Murugeasan, R. *J. Chem. Crystallogr.* **1999**, *29*, 413−420.

(46) Quintal, S. M. O.; Nogueira, H. I. S.; Felix, V.; Drew, M. G. B., *New J. Chem.* **2000**, *24*, 511−517.

(47) Allen, F. H. *Acta Cryst.* **2002**, *B58*, 380−388.

(48) Gavrilova, A. L.; Bosnich, B. *Chem. Rev.* **2004**, *104*, 349−383.

(49) Desiraju, G. R.; Steiner T. The Weak Hydrogen Bond, IUCr Monographs on Crystallography, Oxford Science Publications, 1999.

(50) Ormson, S.M.; Brown, R.G. *Prog. React. Kinet*. **1994**, 19, 45-91.

(51) LeGourrierec, D.; Ormson, S.M.; Brown, R.G. *Prog. React. Kinet*. **1994**, 19, 211-275.

(52) Formosinho, S.J.; Arnaut, L.G.; *J. Photochem. Photobiol. A* **1993**, 75, 21-48.

(53) Dapporto, P.; Formica, M.; Fusi, V.; Giorgi, L.; Micheloni, M.; Paoli, P.; Pontellini, R.; Rossi, P. Inorg. Chem. **2001**, *40*, 6186-6192.

(54) Ambrosi, G.; Formica, M.; Fusi, V.; Giorgi, L.; Macedi, E.; Micheloni, Pontellini, R. *Inorg. Chim*. *Acta* **2009**, 2667−2677.

(55) Ambrosi, G.; Ciattini, S.; Formica, M.; Fusi, V.; Giorgi, L.; Macedi, E.; Micheloni, M.; Paoli, P.; Rossi, P.; Zappia, G. *Chem. Comm*. 2009, 7039−7041.

(56) Fusi, V.; Giorgi, L.; Formica, M.; Micheloni, M.; Macedi, E.; Ambrosi, G.; Paoli, P.; Rossi, P.; Pontellini, R. *Inorg. Chem*. 2009, *49*, 9940−9948.

(57) Torelli, S.; Belle, C.; Gautier-Luneau, I.; Pierre, J. L.; Saint-Aman, E.; Latour, J. M.; Le Pape, L.; Luneau, D. *Inorg. Chem.* **2000**, *39*, 3526−3536.

(58) Koval, I. A.; Huisman, M.; Stassen, A. F.; Gamez, P.; Lutz, M.; Spek, A. L. Pursche, D.; Krebs, B. and Reedijk, J. *Inorg. Chim. Acta*, **2004**, *357*, 294−300.

(59) Koval, I. A.; Huisman, M.; Stassen, A. F.; Gamez, P.; Lutz, M.; Spek, A. L.; Reedijk, J. *Eur. J. Inorg. Chem.* **2004**, 591−600.

(60) Chia, Y.Y.; Tay, M.G. *Dalton. Trans*. **2014**, *43*, 13159−13168.

(61) Klyne, W.; Prelog, V. *Experientia* **1960**, *16*, 521–523.

Table 1. Crystallographic data and refinement parameters for compounds [Ni(H_{-2}**L**)·2(*n*-BuOH)] (**4**), [Ni(H_{-2}**L**)·2(MeOH)] (**5**), [Cd(H_{-2}**L**)·2(DMF)] (**6**), [Cu(H_{-2}**L**)(DMF)] (**7**) and [Pd(H_{-2}**L**)(DMF)] (**8**).

	4	**5**	**6**
Empirical formula	$C_{38}H_{50}N_2NiO_6$	$C_{32}H_{38}N_2NiO_6$	$C_{36}H_{44}CdN_4O_6$
Formula weight	689.51	605.35	741.15
Temperature (K)	150	150	150
Wavelength (Å)	0.71073	0.71073	0.71073
Crystal system, space group	Monoclinic, C2/c	Monoclinic, C2/c	Orthorhombic, $P2_12_12_1$
Unit cell dimensions (Å, °)	a = 15.5622(8) b = 21.2642(6), β= 123.330(7) c = 12.4986(6)	a = 19.941(1) b = 13.0600(5), β= 115.199(7) c = 12.834(7)	a = 11.4735(3) b = 16.7897(5) c = 17.6792(5)
Volume ($Å^3$)	3455.7(3)	3024(2)	3405.7(2)
Z, Dc (mg/cm^3)	4, 1.325	4, 1.330	4, 1.445
μ(mm-1)	0.610	0.687	0.692
F(000)	1472	1280	1536
Crystal size (mm)	0.32x0.28x0.20	0.25x0.20x0.18	0.38x0.32x0.27
θ range (°)	4.230 to 29.180	4.385 to 29.403	4.212 to 29.535
Reflections collected / unique	13616 / 4104	11878 / 3632	31102 / 8293
Data / parameters	4104 / 352	3632 / 243	8293 / 434
Goodness-of-fit on F^2	1.038	1.083	1.090
Final R indices [I>2σ(I)]	R1 = 0.0356, wR2 = 0.0769	R1 = 0.0483, wR2 = 0.0862	R1 = 0.0502, wR2 = 0.0857

R indices (all data)	R1 = 0.0487, wR2 = 0.0843	R1 = 0.0781, wR2 = 0.0962	R1 = 0.0816, wR2 = 0.0974

	7	**8**
Empirical formula	$C_{33}H_{37}N_3CuO_5$	$C_{33}H_{37}N_3PdO_5$
Formula weight	619.19	662.05
Temperature (K)	150	150
Wavelength (Å)	0.71073	0.71073
Crystal system, space group	Monoclinic, $P2_1/n$	Monoclinic, $P2_1/c$
Unit cell dimensions (Å, °)	a = 12.8990(5) b = 9.9207(4), β= 101.279(4) c = 23.3588(9)	a = 10.7317(6) b = 11.6234(5), β= 102.803(5) c = 24.027(1)
Volume ($Å^3$)	2931.4(2)	2922.5(3)
Z, Dc (mg/cm^3)	4, 1.403	4, 1.505
μ(mm-1)	0.792	0.682
F(000)	1300	1368
Crystal size (mm)	0.27x0.23x0.21	0.31x0.28x0.19
θ range (°)	4.151 to 25.443	4.183 to 28.846
Reflections collected / unique	16132 / 4818	12418 / 6388
Data / parameters	4818 / 428	6388 / 490
Goodness-of-fit on F^2	1.076	1.031
Final R indices [I>2σ(I)]	R1 = 0.0461, wR2 = 0.1045	R1 = 0.0439, wR2 = 0.0899
R indices (all data)	R1 = 0.0713, wR2 = 0.1182	R1 = 0.0676, wR2 = 0.1031

Table 2. Selected bond distances (Å) and angles (°) for compounds [Ni(H_{-2}**L**)·2(*n*-BuOH)] (**4**), [Ni(H_{-2}**L**)·2(MeOH)] (**5**), [Cd(H_{-2}**L**)·2(DMF)] (**6**), [Cu(H_{-2}**L**)(DMF)] (**7**) and [Pd(H_{-2}**L**)(DMF)] (**8**)

	4	**5**	**6**	**7**	**8**
M-N(1)	2.113(2)	2.118(2)	2.369(5)	2.035(3)	2.022(3)
M-N(2)			2.362(5)	1.996(3)	2.022(3)
M-O(1)	2.0558(9)	2.062(2)	2.260(4)	1.906(2)	2.009(2)
M-O(3)			2.274(4)	1.927(2)	2.001(2)
M-O(1X)[a]	2.077(2)	2.066(2)	2.282(4)	2.262(3)	
M-O(2X)[b]			2.292(4)		

[a]: M-O(1X) = O(1b) in **4**; O(1m) in **5**; O(1d) in **6**; O(1s) in **7**; [b]: M-O(2X) = O(2d) in **8**

	4	**5**	**6**	**7**	**8**
O(1)-M-N(1)	90.74(5)	89.38(7)	84.0(2)	93.1(1)	91.9(1)
O(1)-M-N(2)			101.0(2)	166.8(1)	178.7(1)
O(1)-M-O(3)			176.5(1)	85.8(1)	87.5(1)
O(1)-M-O(1X)[a]	90.24(5)	85.64(7)	89.4(1)	96.0(1)	
O(1)-M-O(2X)[b]			90.4(2)		
O(3)-M-N(1)			95.9(2)	166.7(1)	178.4(1)
O(3)-M-N(2)			82.4(2)	90.4(1)	93.0(1)
O(3)-M-O(1X)[a]			87.2(1)	93.9(1)	
O(3)-M-O(2X)[b]			90.3(2)		
N(1)-M-O(1X)[a]	177.91(6)	92.75(8)	101.5(2)	99.5(1)	
N(1)-M-O(2X)[b]			167.8(2)		
N(1)-M-N(2)			79.1(2)	99.5(1)	87.7(1)
N(2)-M-O(1X)[a]			169.6(2)	96.9(1)	
N(2)-M-O(2X)[b]			91.4(2)		
O(1X)[a]-M-O(2X)[b]			89.2(2)		

[a]: O(1X) = O(1b) in **4**; O(1m) in**5**; O(1d) in **6**; O(1s) in **7**; [b]: O(2X) = O(2d) in **8**

Table 3. Dihedral angle conformations [61] of the main chain of $[H_{-1}\mathbf{L}]^{2-}$ in compounds $[Ni(H_{-2}\mathbf{L})\cdot 2(n\text{-BuOH})]$ (**4**), $[Ni(H_{-2}\mathbf{L})\cdot 2(MeOH)]$ (**5**), $[Cd(H_{-2}\mathbf{L})\cdot 2(DMF)]$ (**6**), $[Cu(H_{-2}\mathbf{L})(DMF)]$ (**7**) and $[Pd(H_{-2}\mathbf{L})(DMF)]$ (**8**). The dihedral angles are defined by the atoms marked with an asterisk.

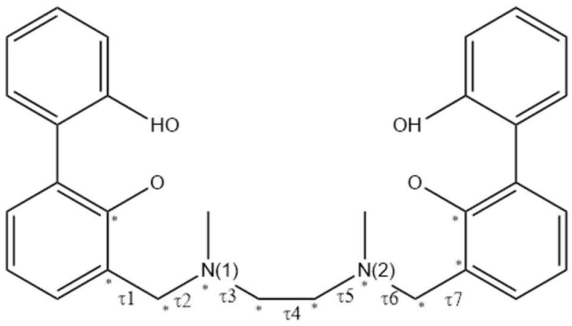

	τ1	τ2	τ3	τ4	τ5	τ6	τ7
4	+sc	+sc	−sc	−sc	−sc	+sc	+sc
5	+sc	+sc	−sc	−sc	−sc	+sc	+sc
6	−sc	ap	−sc	−sc	−sc	ap	−sc
7	−sc	ap	ap	+sc	+sc	ap	+sc
8	−sc	ap	ap	+sc	ap	ap	−sc

Table 4. Selected H-bond interactions in [Ni(H_{-2}**L**)·2(*n*-BuOH)] (**4**), [Ni(H_{-2}**L**)·2(MeOH)] (**5**), [Cd(H_{-2}**L**)·2(DMF)] (**6**), [Cu(H_{-2}**L**)(DMF)] (**7**) and [Pd(H_{-2}**L**)(DMF)] (**8**)

	X-H···Y	X···Y (Å)	H···Y (Å)	X-H···Y (°)
4	O(2)-H(2O)···O(1)	2.494(2)	1.60(2)	166(2)
	O(1b)-H(1ob)···O(2)[a]	2.772(2)	1.94(2)	169(3)

[a] x−1/2,−y+1/2+1,+z−1/2

	X-H···Y	X···Y (Å)	H···Y (Å)	X-H···Y (°)
5	O(2)-H(2O)···O(1)	2.450(3)	1.52(3)	164(3)
	O(1m)-H(1om)···O(2)[b]	2.687(3)	1.85(3)	169(3)

[b] −x,−y,−z+1

	X-H···Y	X···Y (Å)	H···Y (Å)	X-H···Y (°)
6	O(2)-H(2O)···O(1)	2.541(6)	1.68(7)	167(7)
	O(4)-H(4o)···O(3)	2.457(6)	1.65(5)	161(4)

	X-H···Y	X···Y (Å)	H···Y (Å)	X-H···Y (°)
7	O(2)-H(2O)···O(1)	2.508(3)	1.80(4)	165(4)
	O(4)-H(4o)···O(3)	2.530(4)	1.70(5)	166(4)

	X-H···Y	X···Y (Å)	H···Y (Å)	X-H···Y (°)
8	O(2)-H(2O)···O(1)	2.544(3)	1.71(4)	161(4)
	O(4)-H(4o)···O(3)	2.576(3)	1.65(4)	158(4)

Table 5. Basicity constants (log *K*) of **L** determined in 50/50 v/v H_2O/EtOH with 0.15 mol dm^{-3} NMe_4Cl at 298.1 K.

Reaction	**log *K***
$H_{-2}\mathbf{L}^{2-} + H^+ = H_{-1}\mathbf{L}^-$	10.92(1)[a]
$H_{-1}\mathbf{L}^- + H^+ = \mathbf{L}$	8.00(1)
$\mathbf{L} + H^+ = H\mathbf{L}^+$	6.29(1)
$H\mathbf{L}^+ + H^+ = H_2\mathbf{L}^{2+}$	4.49(1)

[a]Values in parentheses are the standard deviations on the last significant figure.

Table 6. Addition constants (log *K*) of metal ions to **L** species determined in 50/50 v/v H_2O/EtOH with 0.15 mol dm^{-3} NMe_4Cl at 298.1 K.

Reaction	**log *K***		
	Ni	**Cu**	**Zn**
$H_{-2}\mathbf{L}^{2-} + M^{2+} = MH_{-2}\mathbf{L}$	14.42(1)	18.55(1)	12.06(1)
$MH_{-2}\mathbf{L} + H^{+} = MH_{-1}\mathbf{L}^{+}$		2.62(1)	5.06(1)
$MH_{-2}\mathbf{L} + 2H^{+} = M\mathbf{L}^{2+}$	9.38(2)		
$MH_{-2}\mathbf{L} + M^{2+} = M_2H_{-2}\mathbf{L}^{2+}$		2.90(2)	
$MH_{-2}\mathbf{L} = MH_{-3}\mathbf{L}^{-} + H^{+}$		−12.35(2)	
$M_2H_{-2}\mathbf{L}^{2+} = M_2H_{-3}\mathbf{L}^{+} + H^{+}$		−5.12(2)	
$M_2H_{-3}\mathbf{L}^{+} = M_2H_{-4}\mathbf{L} + H^{+}$		−10.49(2)	
$M_2H_{-4}\mathbf{L} + OH^{-} = M_2H_{-4}\mathbf{L}(OH)^{-}$		3.54(2)	
$M_2H_{-4}\mathbf{L}(OH)^{-} + OH^{-} = M_2H_{-4}\mathbf{L}(OH)_2^{2-}$		2.65(2)	

[a]Values in parentheses are the standard deviations on the last significant figure.

Scheme 1. Synthesis of ligand **L**

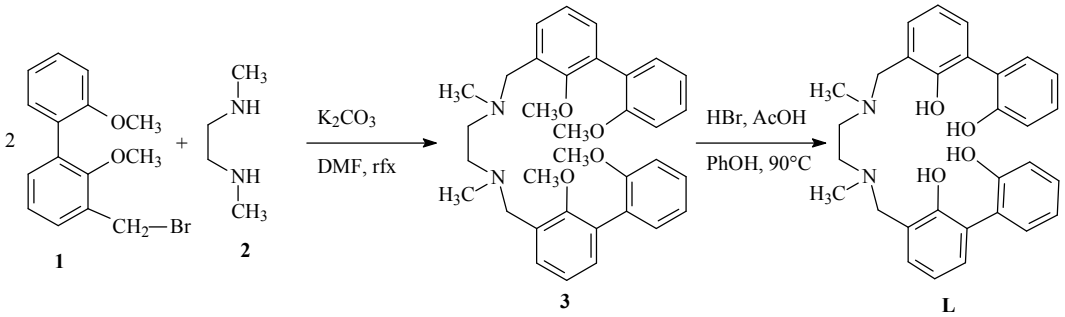

Scheme 2. Proposed location of acidic hydrogen atoms in the protonated species of **L**

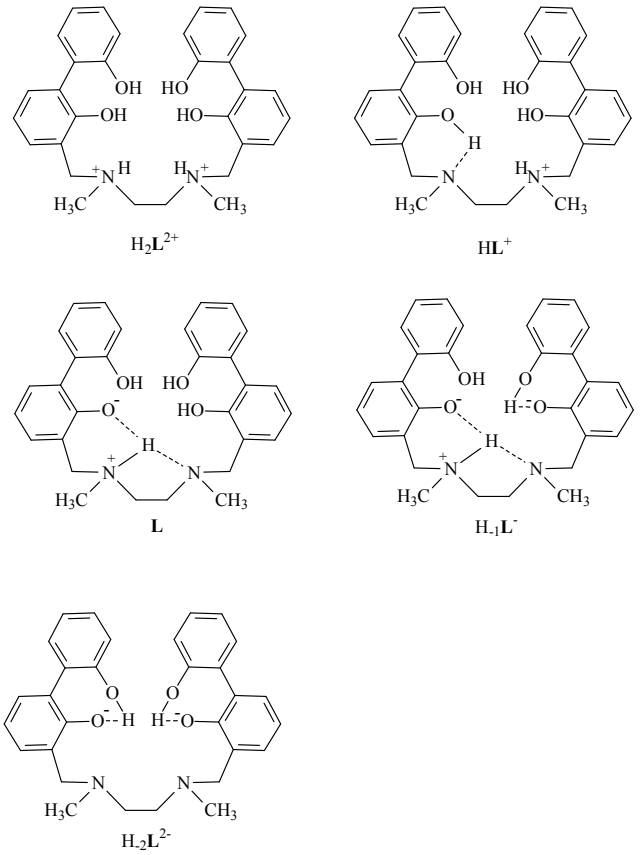

Chart 1. Structure of ligand **L** with labels for the NMR experiments.

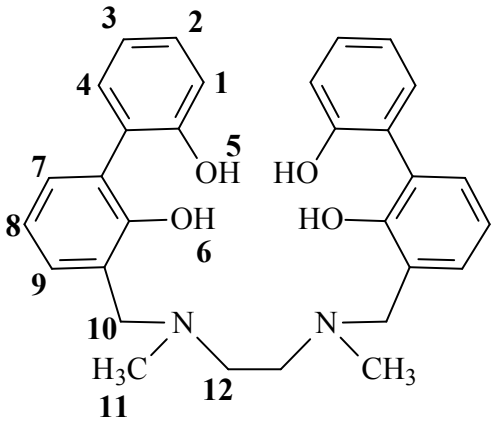

Figure 1. ORTEP 3 view of the complex [Ni(H_{-2}**L**)·2(*n*-BuOH)] (**4**) with the labelling scheme. Ellipsoids are drawn at the 20% probability. Hydrogen atoms (with the exception of the hydroxyl ones) were omitted for clarity.

Figure 2. ORTEP 3 view of the complex [Ni(H_{-2}**L**)·2(MeOH)] (**5**) with the labelling scheme. Ellipsoids are drawn at the 20% probability. Hydrogen atoms (with the exception of the hydroxyl ones) were omitted for clarity.

Figure 3. ORTEP 3 view of the complex [Cd(H_{-2}**L**)·2(DMF)] (**6**) with the labelling scheme. Ellipsoids are drawn at the 20% probability. Hydrogen atoms (with the exception of the hydroxyl ones) were omitted for clarity.

Figure 4. ORTEP 3 view of the complex [Cu(H_{-2}**L**)(DMF)] (**7**) with the labelling scheme. Ellipsoids are drawn at the 20% probability. Hydrogen atoms (with the exception of the hydroxyl ones) were omitted for clarity.

Figure 5. ORTEP 3 view of the complex [Pd(H_{-2}**L**)(DMF)] (**8**) with the labelling scheme. Ellipsoids are drawn at the 20% probability. Hydrogen atoms (with the exception of the hydroxyl ones) were omitted for clarity.

Figure 6. Superimposition of: a) [Ni(H_{-2}**L**)·2(*n*-BuOH)] (**4**) (blue) and [Ni(H_{-2}**L**)·2(MeOH)] (**5**) (green); b) [Ni(H_{-2}**L**)·2(*n*-BuOH)] (**4**) (blue), [Ni(H_{-2}**L**)·2(MeOH)] (**5**) (green) and [Cd(H_{-2}**L**)·2(DMF)] (**6**) (red); c) [Pd(H_{-2}**L**)(DMF)] (**8**) (orange) and [Cu(H_{-2}**L**)(DMF)] (**7**) (pink).

Figure 7. Discovery Studio 4.0 representation of [Ni(H_{-2}**L**)·2(*n*-BuOH)] (**4**) (blue), [Ni(H_{-2}**L**)·2(MeOH)] (**5**) (green), [Cd(H_{-2}**L**)·2(DMF)] (**6**) (red), [Cu(H_{-2}**L**)(DMF)] (**7**) (pink) and [Pd(H_{-2}**L**)(DMF)] (**8**) (orange).

Figure 8. Absorption values at λ=313 nm (♦), relative emission intensity at 401 nm (●), distribution diagram of the protonated species (−) and calculated trend of the fluorescence quantum yield (▬) of **L** as a function of pH in 50/50 v/v ethanol/water solution with 0.15 M Me_4NCl at 298.1 K ([**L**]=10^{-5} M).

Figure 9. Selected ^{1}H-NMR chemical shifts of **L** in D_2O/CD_3OD 50/50 v/v as a function of pH (▼=H8, ▲=H10, ●=H12, ■=H11, see Chart 1).

Figure 10. UV–vis and fluorescence titration of **L** with Zn(II), Cd(II) and Ni(II) solution in 50/50 v/v H_2O/EtOH at pH=7.4 (HEPES) at 298.1 K. [**L**]=$5\cdot10^{-6}$ M, [M(II)] from 0 to $2.5\cdot10^{-5}$ M), emission spectra were acquired by exciting at the isosbestic points (λ_{ex} = 283 nm (Zn), 292 nm (Cd) and 295 nm (Ni)).

Figure 11. Distribution diagrams of **L** in the presence of metal ions (−) and relative emission intensity of Zn(II)/**L** system at 401 nm (λ_{ex}=290 nm) (●) as a function of pH in 50/50 v/v ethanol/water solution with 0.15 M Me_4NCl at 298.1 K. [**L**]=0.001 M, [Ni^{2+}]=0.001 M (**a**), [Cu^{2+}]=0.002 M (**b**), [Cu^{2+}]=0.001 M (**c**), [Zn^{2+}]=0.001 M (**d**).

Figure 12. UV–vis and fluorescence titration of **L** with Cu(II) and Pd(II) solution in

50/50 v/v H_2O/EtOH at pH=7.4 (HEPES) at 298.1 K. [**L**]=$5 \cdot 10^{-6}$ M, [M(II)] from 0 to $2.5 \cdot 10^{-5}$ M), emission spectra were acquired by exciting at λ_{ex} = 320 nm.

Figure 1.

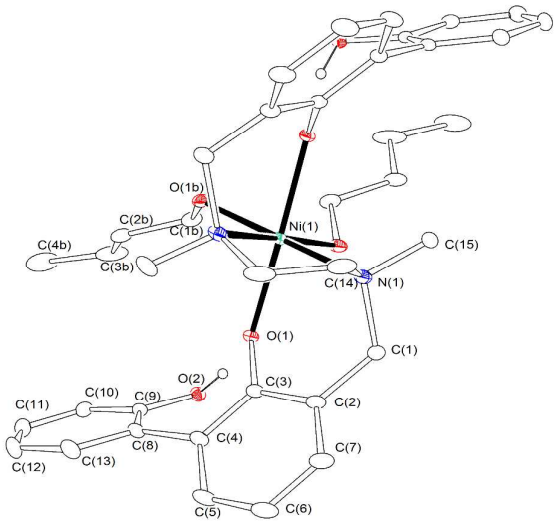
O(1b)
C(2b)
C(1b)
Ni(1)
C(4b)
C(3b)
C(15)
C(14)
N(1)
O(1)
C(1)
O(2)
C(3)
C(10)
C(9)
C(2)
C(11)
C(4)
C(8)
C(7)
C(12)
C(13)
C(5)
C(6)

Figure 2.

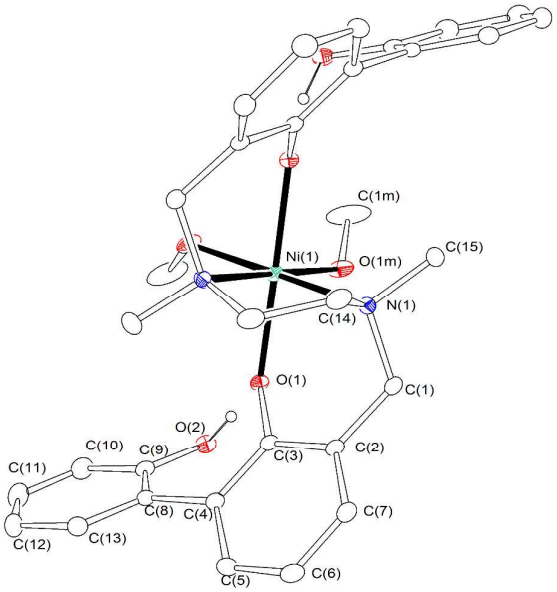
C(1m)
Ni(1)
O(1m)
C(15)
N(1)
C(14)
O(1)
C(1)
O(2)
C(10)
C(9)
C(3)
C(2)
C(11)
C(8)
C(4)
C(7)
C(12)
C(13)
C(5)
C(6)

Figure 3.

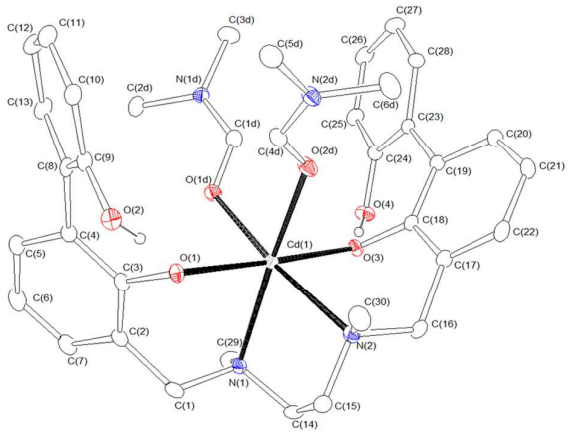
C(12)
C(11)
C(3d)
C(27)
C(5d)
C(26)
C(28)
C(10)
N(1d)
N(2d)
C(2d)
C(6d)
C(13)
C(1d)
C(25)
C(23)
C(20)
C(4d)
O(2d)
C(24)
C(8)
C(9)
C(19)
C(21)
O(1d)
O(4)
O(2)
C(18)
C(22)
C(4)
Cd(1)
C(5)
O(1)
O(3)
C(3)
C(17)
C(6)
C(30)
C(16)
C(2)
C(29)
N(2)
C(7)
N(1)
C(1)
C(15)
C(14)

Figure 4.

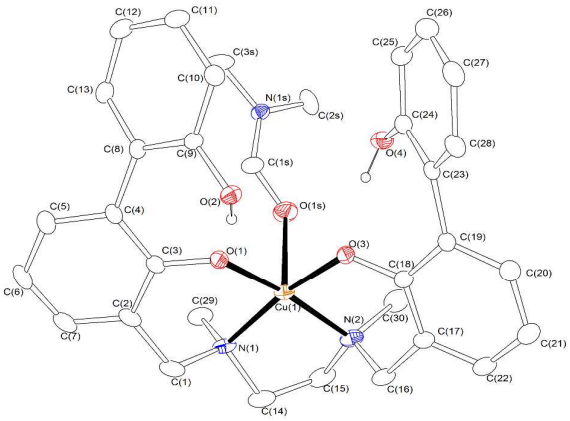
C(12)
C(11)
C(3s)
C(10)
C(13)
N(1s)
C(2s)
C(8)
C(9)
C(1s)
O(2)
O(1s)
C(5)
C(4)
C(3)
O(1)
O(3)
C(6)
C(2)
C(29)
Cu(1)
N(2)
C(30)
C(7)
N(1)
C(1)
C(15)
C(16)
C(14)
C(26)
C(25)
C(27)
C(24)
C(28)
O(4)
C(23)
C(19)
C(18)
C(20)
C(17)
C(21)
C(22)

Figure 5.

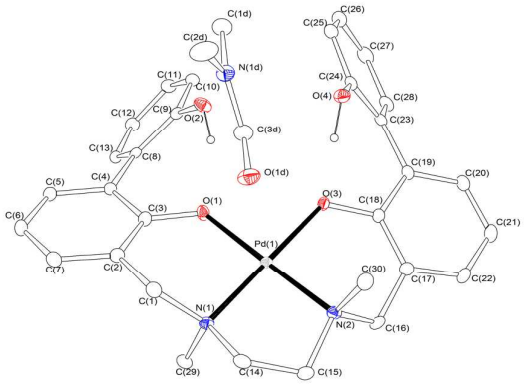
C(1d)
C(2d)
N(1d)
C(11)
C(10)
C(12)
C(9)
O(2)
C(3d)
C(13)
C(8)
O(1d)
C(5)
C(4)
C(6)
C(3)
O(1)
O(3)
C(18)
Pd(1)
C(7)
C(2)
C(30)
C(1)
N(1)
N(2)
C(16)
C(29)
C(14)
C(15)
C(26)
C(25)
C(27)
C(24)
O(4)
C(28)
C(23)
C(19)
C(20)
C(21)
C(17)
C(22)

Figure 6.

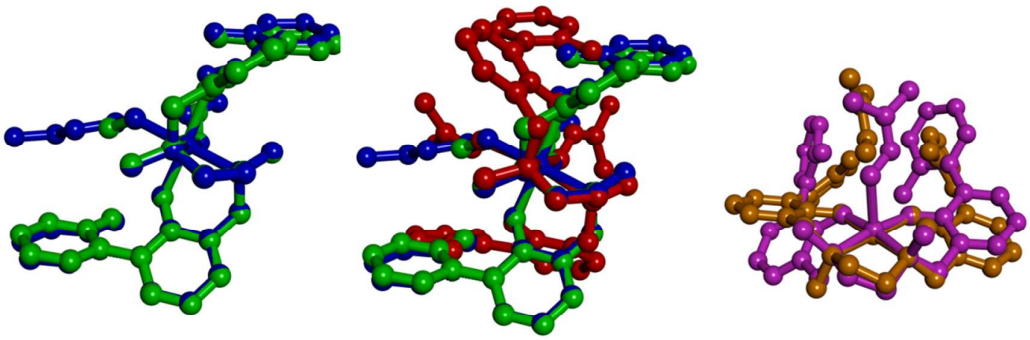

a b c

Figure 7.

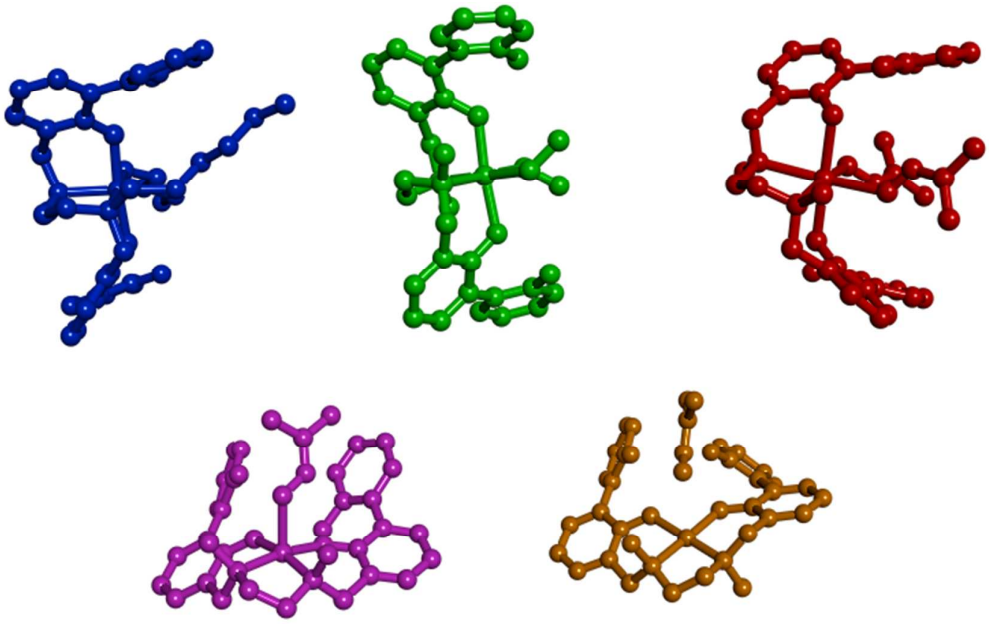

Figure 8.

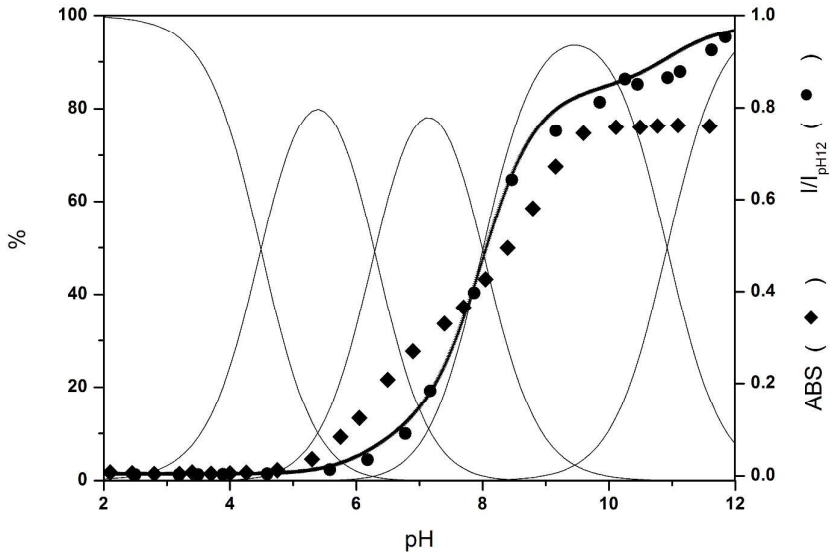

Figure 9.

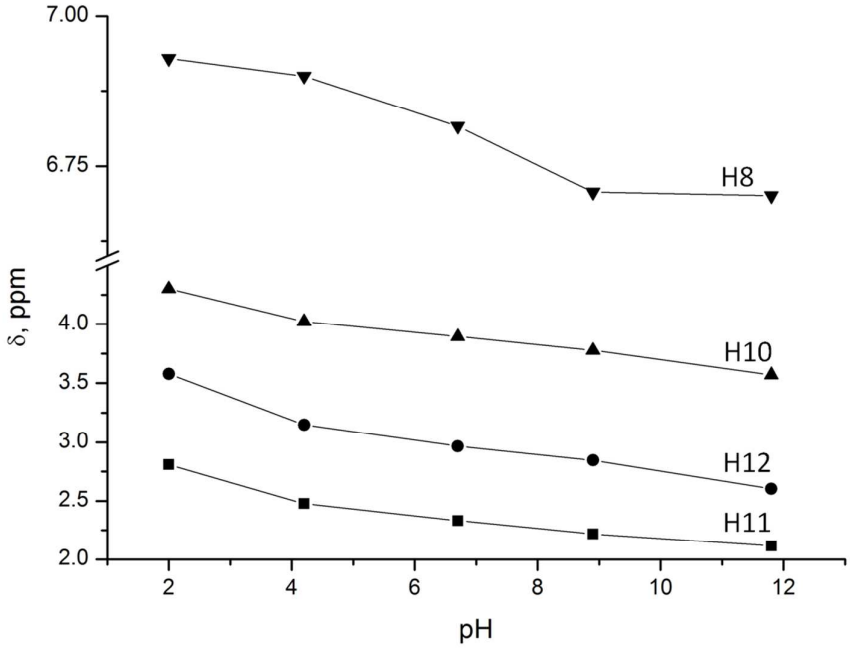

Figure 10.

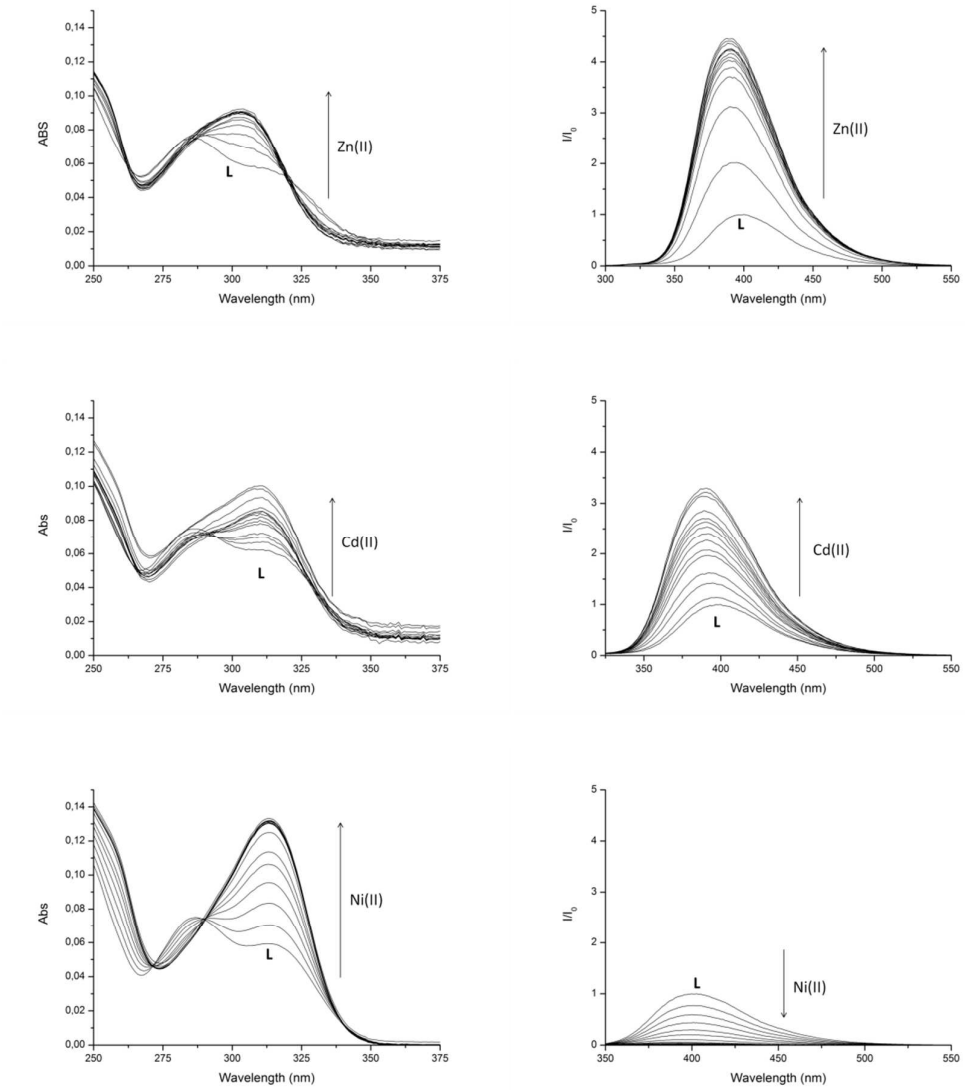
ABS
Zn(II)
L
Wavelength (nm)
I/I0
Zn(II)
L
Wavelength (nm)
Abs
Cd(II)
L
Wavelength (nm)
I/I0
Cd(II)
L
Wavelength (nm)
Abs
Ni(II)
L
Wavelength (nm)
I/I0
L
Ni(II)
Wavelength (nm)

Figure 11.

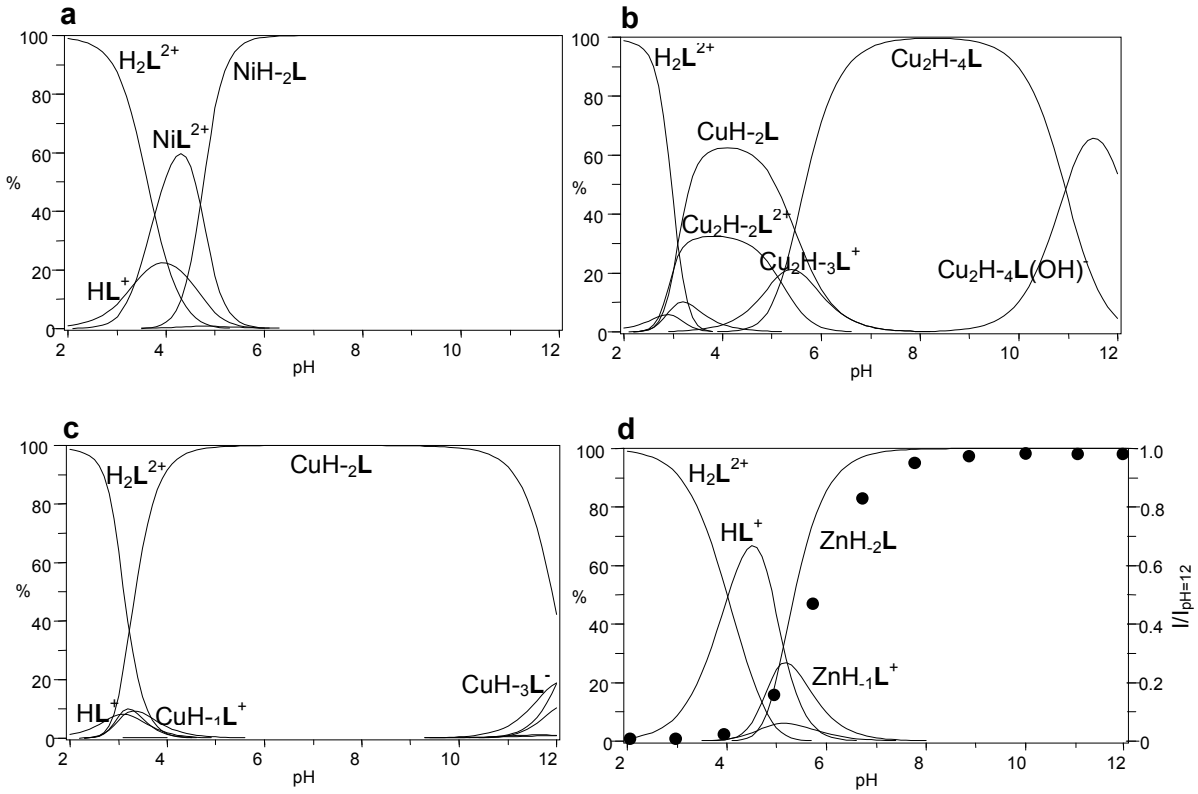
a
H_2L^{2+}
$NiH_{-2}L$
NiL^{2+}
HL^{+}
%
pH
b
H_2L^{2+}
$Cu_2H_{-4}L$
$CuH_{-2}L$
$Cu_2H_{-2}L^{2+}$
$Cu_2H_{-3}L^{+}$
$Cu_2H_{-4}L(OH)^{-}$
%
pH
c
H_2L^{2+}
$CuH_{-2}L$
$CuH_{-3}L^{-}$
HL^{+}
$CuH_{-1}L^{+}$
%
pH
d
H_2L^{2+}
HL^{+}
$ZnH_{-2}L$
$ZnH_{-1}L^{+}$
%
pH
$I/I_{pH=12}$

Figure 12.

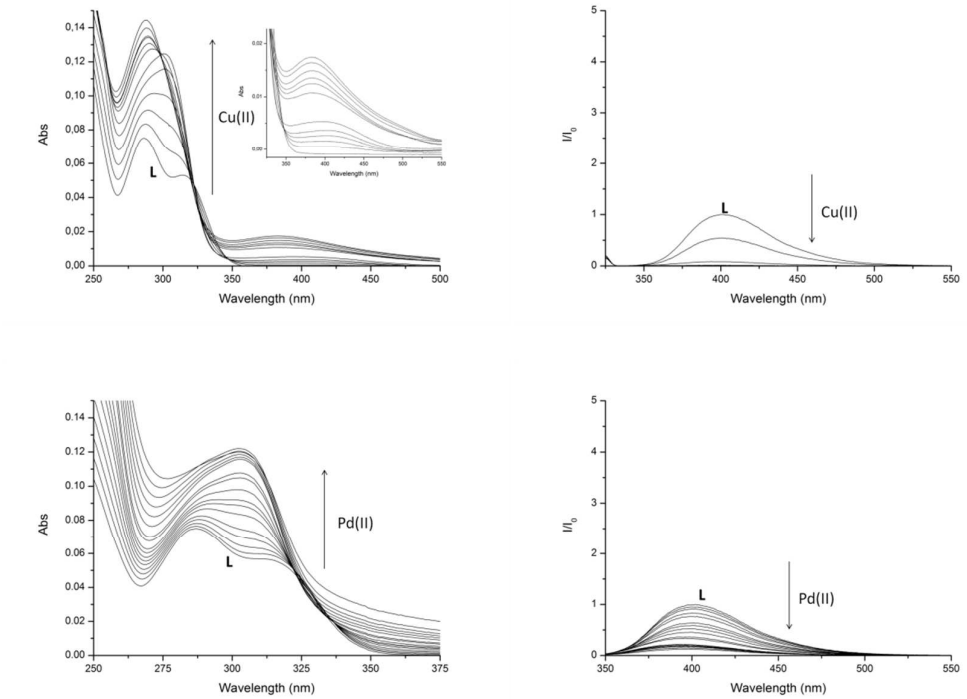

Table of content-synopsis

The coordination properties towards Ni(II), Cu(II), Zn(II), Cd(II) and Pd(II) of the ligand N,N'-Bis[(2,2'-dihydroxybiphen-3-yl)methyl]-N,N'-dimethylethylenediamine (**L**), containing two biphenol moieties (BPH) as coordinating and photoactive unit linked to ethylenediamine scaffold, were studied in ethanol/water solution. The ligand behaves as a fluorescent OFF-ON sensor for Zn(II) and Cd(II) at physiological pH. The coordination of these metal ions produces an intense blue emission observable with the naked-eye.